energies

MDPI

Article

An Efficiency Enhancement Technique for a Wireless Power Transmission System Based on a Multiple Coil Switching Technique

Vijith Vijayakumaran Nair and Jun Rim Choi*

School of Electronics Engineering, Kyungpook National University, Buk-gu, Daegu 702-701, Korea; vijith133@knu.ac.kr

* Correspondence: jrchoi@ee.knu.ac.kr; Tel.: +82-053-940-8567; Fax: +82-053-954-6857

Academic Editor: Jihong Wang
Received: 15 October 2015; Accepted: 29 January 2016; Published: 3 March 2016

Abstract: For magnetic-coupled resonator wireless power transmission (WPT) systems, higher power transfer efficiency can be achieved over a greater range in comparison to inductive-coupled WPT systems. However, as the distance between the two near-field resonators varies, the coupling between them changes. The change in coupling would in turn vary the power transfer efficiency. Generally, to maintain high efficiency for varying distances, either frequency tuning or impedance matching are employed. Frequency tuning may not limit the tunable frequency within the Industrial Scientific Medical (ISM) band, and the impedance matching network involves bulky systems. Therefore, to maintain higher transfer efficiency over a wide range of distances, we propose a multiple coil switching wireless power transmission system. The proposed system includes several loop coils with different sizes. Based on the variation of the distance between the transmitter and receiver side, the power is switched to one of the loop coils for transmission and reception. The system enables adjustment of the coupling coefficient with selective switching of the coil loops at the source and load end and, thus, aids achieving high power transfer efficiency over a wide range of distances. The proposed technique is analyzed with an equivalent circuit model, and simulations are performed to evaluate the performance. The system is validated through experimental results that indicate for a fixed frequency (13.56 MHz) that the switched loop technique achieves high efficiency over a wider range of distances.

Keywords: wireless power transmission; magnetically-coupled resonators; coupling coefficient tuning; power transfer efficiency

1. Introduction

Advances in wireless power transmission (WPT) technology have remarkably facilitated the rapid development of mobile electronic devices, biomedical devices, industrial, automotive and space satellite applications. In general WPT techniques are classified into three types [1] based on the transmission techniques: (1) the electromagnetic (EM) radiation technique, which transmits microwave energy over long distances and is used for space satellite applications [1]; (2) the inductive coupling technique, which allows the transfer of energy over very short distances and is used in wireless charging applications, such as laptops, mobile phones and biomedical implants [1–5]. For energy harvesting applications, the work presented in [6] depicted long-range energy transfer based on inductive coupling for a distance of 6 m, but the power received was confined to 10.9 mW for a 246-W DC power input. Further, in [7], a designed and fabricated inductive power transfer system displayed higher efficiency of 77% at a distance of 30 cm. The work showed effective improvement in achieving power transfer efficiency for a longer range, but beyond 30 cm, the

efficiency decreased gradually. Therefore, for short-range power transfer, the inductive coupling method is usually employed. However, as the distance range increases, the inductive coupling method becomes unsuitable as the power transfer efficiency rapidly decreases. (3) To increase the power transmission range, magnetically-coupled resonance power transfer is proposed in [8,9], which effectively increased the transfer range in comparison to the inductive coupling method. This technique is based on the concept that two resonators with a similar resonance frequency effectively exchange power, and it is widely used in consumer electronics and automotive applications [10–12]. However, in practical systems, power transfer efficiency drops rapidly, when the distance between the coils increases or the coils are misaligned [11,13]. As all of the applications demand a highly efficient end-to-end wireless power delivery system, it is essentially important to consider techniques to achieve optimal efficiency.

To obtain maximum efficiency for a WPT system, several methods have been proposed and studied in prior works [11–21]. These methods consist of adaptive circuits to optimize efficiency based on frequency control, impedance matching control, Q-factor tuning control and adjusting the coupling coefficient. The work in [11] reports a frequency tuning technique to mitigate the effect of frequency splitting and to improve the efficiency of the WPT system. However, the technique violates the frequency standards (Industrial Scientific Medical (ISM) Band) of wireless power transmission as it requires a wide frequency bandwidth. In [12,14–17,22], adaptive impedance matching-based efficiency improvement is proposed. However, the range of tuning to obtain optimal efficiency was limited by the varactors employed in the circuit, and additionally, varactor losses reduced the total efficiency of the system. The work in [13,18–21] details optimizing the efficiency based on varying the coupling between the coils. However, [13,18–20] describes the method based on manually changing the distance between the coils to vary the coupling coefficient and obtain the optimal efficiency, whereas [21] suggests manually misaligning the source coil to vary the coupling coefficient to obtain maximum power transfer efficiency. However, in practical cases, the manual adjustment of the coils is not a viable option to obtain maximum power transfer efficiency.

In this paper, we propose a WPT system based on a controlled switching technique with multiple loop coils to optimize the power transfer efficiency over a wide operational range. This method involves several loop coils with different sizes at the transmitter side and receiver side. The loop coils are adequately selected to adjust the coupling coefficient, so as to obtain the optimum coupling coefficient for achieving maximum power transfer efficiency with varying distance between the transmitter side and receiver side over a wide distance range. The detailed analysis of the system is provided in the following sections. The paper is organized as follows: Section 2 details the analysis of the four-coil WPT system based on a circuit model. Section 3 analyzes the optimization strategy for maximum power transmission efficiency, and the proposed efficiency optimization method is described in Section 4. The simulation and experimental results are discussed in Section 5, followed by the conclusion in Section 6.

2. Magnetic Resonance WPT System

2.1. Four-Coil WPT System

The WPT system proposed in prior work [8], which employed four magnetically-coupled resonators, is depicted in Figure 1. The power from the supply is provided to the source coil (N1 urns), which is transmitted to the magnetically-coupled transmitter coil (Tx) (N2 turns). The Tx coil transfers the energy to the receiver coil (Rx) (N3 turns), which are magnetically coupled to each other. At the receiver side, the load coil (N4 turns) receives the power from the Rx coil, to further supply to the output load. The resonators are designed to have the identical resonant frequency for maximum power transfer. The power transfer efficiency of this system is strongly dependent on the distance between Tx and Rx (d_{23}), and there exists an optimum distance to obtain maximum efficiency [8,9,11].

The efficiency rapidly decreases as the optimum distance varies. The proposed work deals with a technique to obtain maximum efficiency for a wider range of distances at fixed input frequency.

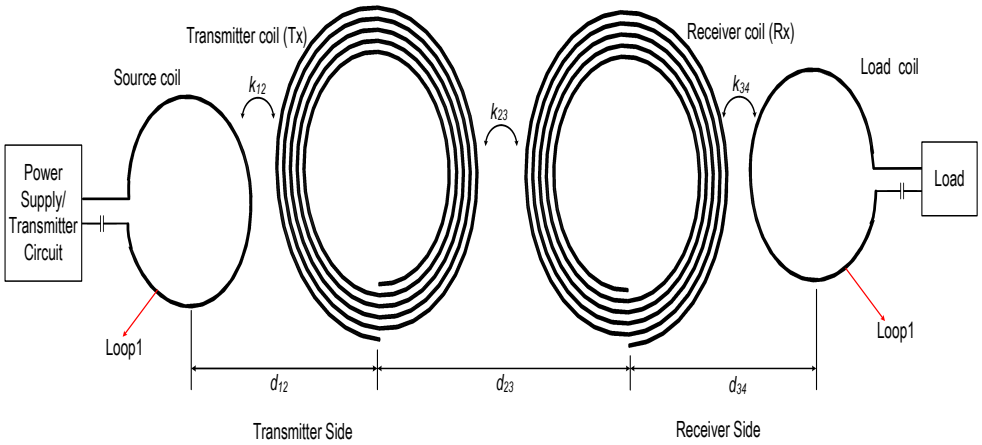

Figure 1. Magnetic resonance-coupled wireless power transmission (WPT) system.

2.2. Analysis Based on Circuit Model

For a detailed analysis of the four-coil WPT system, the system can be modeled as a combination of lumped circuit elements (L, self-capacitance (C) and parasitic resistance (R)) [11]. The equivalent circuit model of the magnetically-coupled resonator system is depicted in Figure 2. Each coil in the system is represented with their corresponding values of self-inductance (L), R and C. The coils are fabricated to resonate at a particular frequency of interest. External capacitors are added to the single-turn source and load coils to make them resonate at the frequency of interest. The coils are linked to each other via a magnetic field, characterized by the coupling coefficients k_{12} (source to Tx), k_{23} (Tx to Rx) and k_{34} (Rx to load). As the cross coupling between the source to Rx coil and Tx to load coil is relatively weak, these coupling factors are neglected for the convenience of the analysis [11,13]. The coupling coefficient between two coils x and y is given by:

$$k_{xy} = \frac{M_{xy}}{\sqrt{L_x L_y}} \tag{1}$$

where M_{xy} is the mutual inductance between the coils x and y and L is the self-inductance of the coils. In Figure 2, by applying Kirchhoff's voltage law (KVL), the relationship between voltage applied to the power coil and currents through each coil is determined based on the following matrix.

$$\begin{bmatrix} V_S \\ 0 \\ 0 \\ 0 \end{bmatrix} = \begin{bmatrix} Z_1 & j\omega M_{12} & 0 & 0 \\ j\omega M_{12} & Z_2 & -j\omega M_{23} & 0 \\ 0 & -j\omega M_{23} & Z_3 & j\omega M_{34} \\ 0 & 0 & j\omega M_{34} & 0 \end{bmatrix} \begin{bmatrix} i_1 \\ i_2 \\ i_3 \\ i_4 \end{bmatrix} \tag{2}$$

where,

$$Z_1 = R_S + R_1 + j\left(\omega L_1 - \frac{1}{\omega C_1}\right) \tag{3}$$

$$Z_2 = R_2 + j\left(\omega L_2 - \frac{1}{\omega C_2}\right) \tag{4}$$

$$Z_3 = R_3 + j\left(\omega L_3 - \frac{1}{\omega C_3}\right) \tag{5}$$

$$Z_4 = R_L + R_4 + j\left(\omega L_4 - \frac{1}{\omega C_4}\right) \tag{6}$$

V_S is voltage applied to the source coil, Z represents the loop impedance of the coils and i indicates the loop current. Solving for current i_4 in the load coil from the matrix in Equation (2), i_4, is given by:

$$i_4 = -\frac{j\omega^3 M_{12} M_{23} M_{34} V_S}{Z_1 Z_2 Z_3 Z_4 + \omega^2 M_{12}^2 Z_3 Z_4 + \omega^2 M_{23}^2 Z_1 Z_4 + \omega^2 M_{34}^2 Z_1 Z_2 + \omega^4 M_{12}^2 M_{34}^2} \tag{7}$$

The voltage across the load resistor R_L is given by:

$$V_L = -i_4 R_L \tag{8}$$

The system can be considered as a two-port network (the input fed from the source as the first port and the output that feeds the load as the second port) and further analyzed based on scattering parameters, as in [23]. The power transmitted is represented in terms of the linear magnitude of the transmission coefficient $|S_{21}|$ and is significant in the analysis, as it can be monitored with a vector network analyzer (VNA) for experimental verification. The parameter S_{21} is calculated as in [11] and is given by:

$$S_{21} = 2\frac{V_L}{V_S}\sqrt{\frac{R_S}{R_L}} \tag{9}$$

Thus substituting Equations (1), (7) and (8) in Equation (9), $|S_{21}|$ is given by:

$$|S_{21}| = \frac{2\omega^3 k_{12} k_{23} k_{34} L_2 L_3 \sqrt{L_1 L_4 R_S R_L}}{Z_1 Z_2 Z_3 Z_4 + k_{12}^2 L_1 L_2 Z_3 Z_4 \omega^2 + k_{23}^2 L_2 L_3 Z_1 Z_4 \omega^2 + k_{34}^2 L_3 L_4 Z_1 Z_2 \omega^2 + k_{12}^2 k_{34}^2 L_1 L_2 L_3 L_4 \omega^4} \tag{10}$$

To further simplify the Equation (10), the quality factor (Q-factor) parameter of the coil is considered. The Q-factor of a coil is represented as:

$$Q_i = \frac{1}{R_i}\sqrt{\frac{L_i}{R_i}} = \frac{\omega_i L_i}{R_i} = \frac{1}{\omega_i C_i R_i} : i = 1 \sim 4; \qquad \omega_i = \frac{1}{\sqrt{L_i C_i}} \tag{11}$$

where ω_i is the self-resonance frequency of the i-th coil and R_i is the equivalent resistance of the i-th coil. The coils are designed to have the same resonant frequency. At resonance condition, the impedance of the coils is given as:

$$Z_1 = R_S + R_1 \approx R_S; \qquad Z_2 = R_2; \qquad Z_3 = R_3; \qquad Z_4 = R_L + R_4 = R_L \tag{12}$$

For simplicity of the analysis, R_S is set equal to R_L. Therefore, for a particular resonant frequency of the system, from Equations (10)–(12), the magnitude of S_{21} can be written as:

$$|S_{21}| = \frac{2k_{12} k_{23} k_{34} Q_2 Q_3 \sqrt{Q_1 Q_4}}{1 + k_{12}^2 Q_1 Q_2 + k_{23}^2 Q_2 Q_3 + k_{34}^2 Q_3 Q_4 + k_{12}^2 k_{34}^2 Q_1 Q_2 Q_3 Q_4} \tag{13}$$

Since, the power transfer efficiency of the designed and fabricated system is to be analyzed, the power transfer efficiency is expressed in terms of the S-parameter. The power transfer efficiency in terms of the S-parameter by definition as in [23] is given by:

$$\eta(\%) = |S_{21}|^2(\%) \tag{14}$$

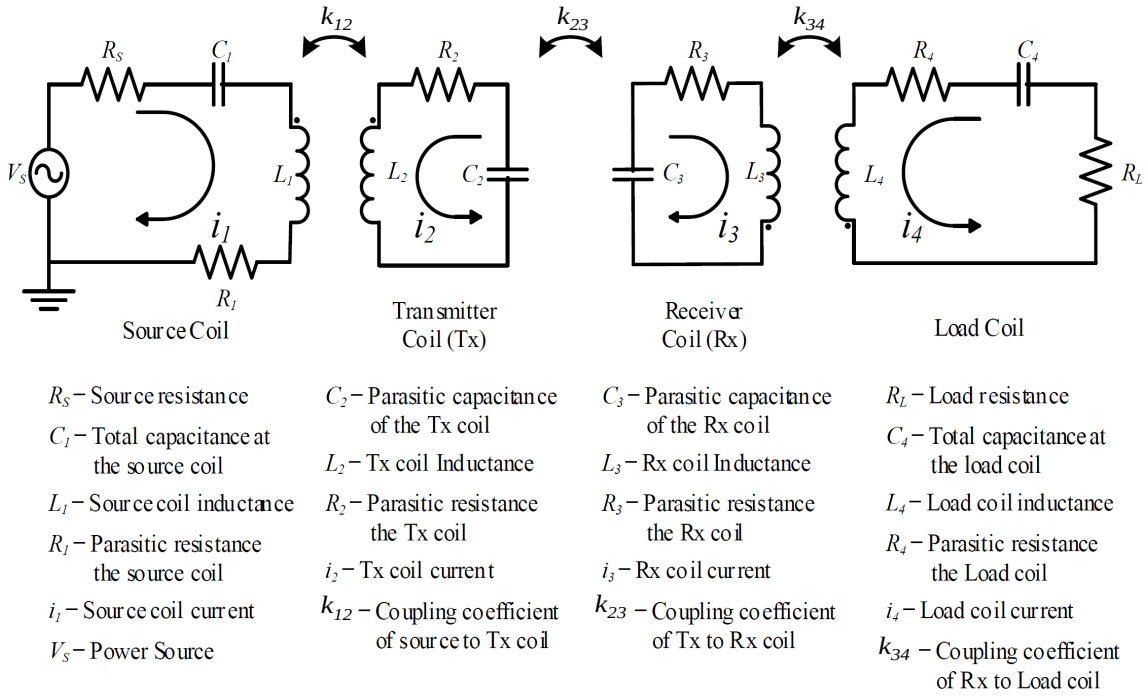

Figure 2. WPT system equivalent circuit model.

3. Optimization of Power Transfer Efficiency

The designed WPT system has to be optimized to achieve maximum power transfer efficiency for a particular range with fixed resonating frequency (13.56-MHz ISM band frequency for our experimental purposes). The Equation (13) implies that the power transfer efficiency is influenced by the coupling factors k_{12}, k_{23} and k_{34} for a given Q_1, Q_2, Q_3 and Q_4. Further, the coupling coefficient is a strong function of the distance between the coils. For symmetric coils, Tx and Rx, with n turns and radius r ($r \ll d_{23}$), the mutual inductance is calculated based on the Neumann formula and is given by:

$$M_{23} \cong \frac{\mu_0 \pi n^2 r^4}{2 d_{23}^3} \tag{15}$$

where μ_0 is the permeability of free space. Hence, for symmetric coils from Equations (1) and (15), k_{23} is evaluated as:

$$k_{23} \cong \frac{\mu_0 \pi n^2 r^4}{2 L d_{23}^3} \tag{16}$$

where $L = L_2 = L_3$ is the self-inductance of each coil. Equation (1) implies that k_{23} is directly proportional to $1/d_{23}^3$, which indicates the dramatic decrease in the efficiency with distance between the coils.

The efficiency can be maximized for a given distance d_{23} and particular resonance frequency, by choosing the optimum value of coupling coefficients k_{12} and k_{34}, as efficiency is a dependent parameter of the coupling coefficients, stated in Equation (13). Two case studies are taken into consideration for the evaluation of the efficiency for a particular distance (d_{23}) between the Tx and Rx with fixed resonant frequency (13.56 MHz). The Tx and Rx coils are assumed to be identical for the analysis. Hence the quality factors of Tx and Rx are equal ($Q_2 = Q_3$).

Case 1: $k_{12} \neq k_{34}$

The efficiency can be maximized for given k_{23} (or d_{23}) and k_{34} by optimizing k_{12}, such that:

$$\frac{\partial |S_{21}|}{\partial k_{12}} = 0 \qquad at \quad k_{12} = k_{12opt} \tag{17}$$

From Equation (17), the optimal value of k_{12opt} is computed as given in Equation (18).

$$k_{12opt} = \sqrt{\frac{1 + k_{23}^2 Q_2^2 + k_{34}^2 Q_2 Q_4}{Q_1 Q_2 + k_{34}^2 Q_1 Q_2^2 Q_4}} \tag{18}$$

Equation (18) is substituted in Equation (13) to obtain optimum $|S_{21}|$ for a given distance.

$$|S_{21opt}| = \frac{2k_{12opt} k_{23} k_{34} Q_2^2 \sqrt{Q_1 Q_4}}{1 + k_{12opt}^2 Q_1 Q_2 + k_{23}^2 Q_2^2 + k_{34}^2 Q_3 Q_4 + k_{12opt}^2 k_{34}^2 Q_1 Q_2^2 Q_4} \tag{19}$$

Case 2: $k_{12} = k_{34}$

For a given k_{23} (or d_{23}) with symmetrical coils, the coupling coefficients $k_{12} = k_{34}$, and the quality factors $Q_2 = Q_3$ and $Q_1 = Q_4$. Based on these conditions, Equation (13) is further simplified, and the magnitude of $|S_{21}|$ is given as:

$$|S_{21}| = \frac{2k_{12}^2 k_{23} Q_1 Q_2^2}{\left(1 + k_{12}^2 Q_1 Q_2\right)^2 + k_{23}^2 Q_2^2} \tag{20}$$

To obtain the optimum k_{12} to maximize the efficiency for a given distance, the procedure in Equation (17) is repeated, and the optimum value k_{12opt} is obtained from Equation (21).

$$k_{12opt} = \left(\frac{k_{23}^2}{Q_1} + \frac{1}{Q_1^2 Q_2^2}\right)^{1/4} \tag{21}$$

Equation (21) is substituted in Equation (20) to obtain optimum $|S_{21}|$ for a given distance and is given by:

$$|S_{21opt}| = \frac{2k_{12opt}^2 k_{23} Q_1 Q_2^2}{\left(1 + k_{12opt}^2 Q_1 Q_2\right)^2 + k_{23}^2 Q_2^2} \tag{22}$$

4. Proposed Efficiency Optimization Method

4.1. Controlled Switching Technique with Multiple Loop Coils

The WPT system is designed and optimized based on the design and optimization method detailed in [24,25]. To maximize the efficiency of WPT for a given distance and fixed resonating frequency, a controlled switching technique with multiple loop coils to determine the optimal k_{12} is proposed. Figure 3 shows the schematic of the proposed switching loop WPT system for two different cases, as explained in Section 4.

Case 1: $k_{12} \neq k_{34}$

For Case 1, the Tx and Rx coils are identical and symmetrical, but the source (loop1, loop2, loop3) and load (loop4) coils are not identical in Figure 3. Three loops at the source end are switched between each other to the power supply for varying d_{23}, for providing power to the load coil. The switching between the loops enables obtaining the optimum k_{12} for a particular d_{23}, which in turn aids achieving the maximum efficiency.

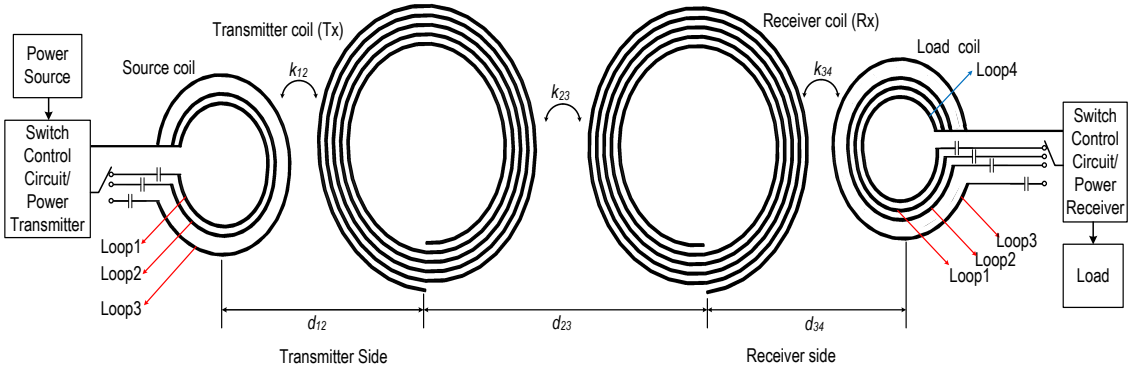

Figure 3. Proposed WPT system with the multiple loop coil switching technique.

Case 2: $k_{12} = k_{34}$

For Case 2, the Tx and Rx coil are identical and symmetrical; also the source (loop1, loop2, loop3) and load (loop1, loop2, loop3) are identical in Figure 3. The loops at the source side and load side are switched simultaneously at both ends of the WPT system for varying d_{23} to obtain k_{12opt}.

4.2. Design and Fabrication of the System

The proposed WPT system is designed and fabricated for the model validation as in Figure 3. Each coil at the source and load is coupled with a series capacitor to make the loop resonate at a 13.56-MHz frequency. The Tx and Rx coils are also carefully designed for the self-inductance and parasitic capacitance that allow the coils to resonate at a 13.56-MHz frequency. The coils are fabricated using copper wire, and the source and load coils are separated from the respective Tx and Rx coils by a distance of 5 mm ($d_{12} = d_{34} = 5$ mm). Table 1 shows the design dimensions of the coils.

Table 1. Structural dimensions of the fabricated coils and loops.

Parameter	Coil1	Coil2	Loop1	Loop2	Loop3	Loop4
Number of turns	5	5	1	1	1	1
Outer diameter (mm)	300	300	125	150	200	100
Inner diameter (mm)	265	265	NA	NA	NA	NA
Pitch (mm)	5	5	NA	NA	NA	NA
Wire diameter (mm)	2	2	2	2	2	2

One of the significant challenges in the fabrication and measurement is to accurately determine the resonance frequency of the coil structure, since it is difficult to predict the parasitic capacitance of the coils. Therefore, the coils are manually trimmed at the end to tune for the resonance frequency. Besides this, for source and load coils, RF Mica capacitors with a low equivalent series resistance (ESR) value are used to connect in series with the coil loop to make the coils resonate at 13.56 MHz. To determine the measurement values, standard radio frequency (RF) and microwave techniques are utilized to extract parameters, such as the coupling coefficient, resonant frequency and Q-factor from resonant coils [23]. The measured parameters of the coils using vector network analyzer (VNA) are depicted in Table 2.

Table 2. Measured parameters of the coils and loops.

Parameter	Coil1	Coil2	Loop1	Loop2	Loop3	Loop4
Inductance (μH)	16.32	16.26	0.468	0.56	0.783	0.35
Capacitance (pF)	8.48	9.2	295	245	181	356
Resonant Frequency (MHz)	13.536	13.547	13.57	13.6	13.562	13.578
Q-factor at Resonance (mm)	463	462	0.87	0.95	1.02	0.83

5. Simulation and Experimental Results

The proposed power transfer efficiency enhancement technique for the WPT system is validated based on simulation and experimental results. From Equations (13), (14) and (16), it is noted that the power transfer efficiency is a strong function of the distance between the Tx and Rx (d_{23}). However, for our design considerations that involve optimization of the power transfer efficiency for various d_{23} at a fixed frequency, Cases 1 and 2 in Section 4 are considered. The proposed work aims at optimizing k_{12} for achieving high efficiency for a particular d_{23} (k_{23}). Since, Equation (16) is an approximated Neumann formula for $r \ll d_{23}$, the original Neumann formula is employed to predict k_{12opt} for a particular d_{23}, as reported in [26–28]. The mutual inductance between the Tx and Rx is computed initially for two single turn loops x and y as given in Equation (23).

$$M_{mn} = \oint_m \oint_n \frac{d\vec{l_m} \cdot d\vec{l_n}}{r} \tag{23}$$

where μ_0 is the permittivity of free space and r is the distance between the incremental lines $d\vec{l_m}$ and $d\vec{l_m}$. For the computation of the mutual inductance of multiple turn coils, with N_1 and N_2 turns, the Equation in (23) is decomposed into sets of N_1 and N_2 closed loops and approximated for M_{total} as in Equation (24) [26–28]. The coupling coefficient is further calculated based on the Equation in (1).

$$M_{total} = \sum_{m=1}^{N_1} \sum_{n=1}^{N_2} M_{mn} \tag{24}$$

In Case 1, for varying d_{23}, the power supply at the source end is switched to one of the three loops, such that k_{12} in Equation (18) is satisfied. k_{12opt} in Equation (18) is calculated as a dependable parameter of d_{23}. Figure 4 shows the computed results for a Case 1-type system. The computed k_{23} as a function of d_{23} based on Equations (1), (23) and (24) is represented in Figure 4 using the measured value of coil parameters as given in the Table 2. Furthermore, the optimal k_{12} for varying d_{23}, derived from Equation (18) for three different loops at the source end (loop1, loop2, loop3) with loop4 as the load coil, is depicted in Figure 4. The obtained k_{12} for each loop is indicated in Figure 4. Loop1 in the system is targeted for $d_{23} = 30$ cm, loop2 for $d_{23} = 35$ cm and loop 4 $d_{23} = 40$ cm. Figure 4 validates that the proposed technique can be used to obtain optimal k_{12} (k_{12opt}) for varying d_{23}.

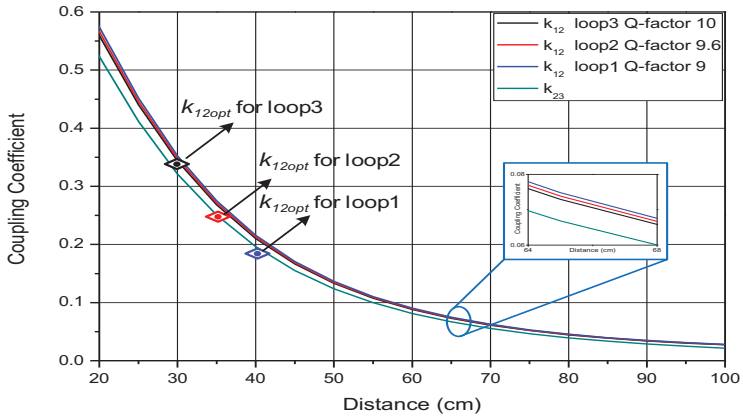

Figure 4. Computed k_{12opt} for the Case 1 system for three different loops and k_{23} for varying d_{23}. The obtained k_{12} for different loops are indicated with three points.

In Case 2, with respect to varying d_{23}, the power supply is switched to one of the three loops at the source end simultaneously with the identical loops at the receiver end, such that k_{12} in Equation (21) is satisfied.

The computed k_{23} with reference to d_{23} is depicted in Figure 5. The different loop coil parameters, as in Table 2, are substituted in Equation (20) and the obtained k_{12opt} with respect to d_{23} is plotted. Furthermore, the obtained k_{12} for each loop is illustrated in Figure 5. Loop1 is intended for $d_{23} = 25$ cm, loop2 for $d_{23} = 35$ cm and loop 4 $d_{23} = 60$ cm. Thus, Figure 5 validates that the proposed Case 2 technique can be used to obtain k_{12opt} for a wider range of distances in comparison to Case 1.

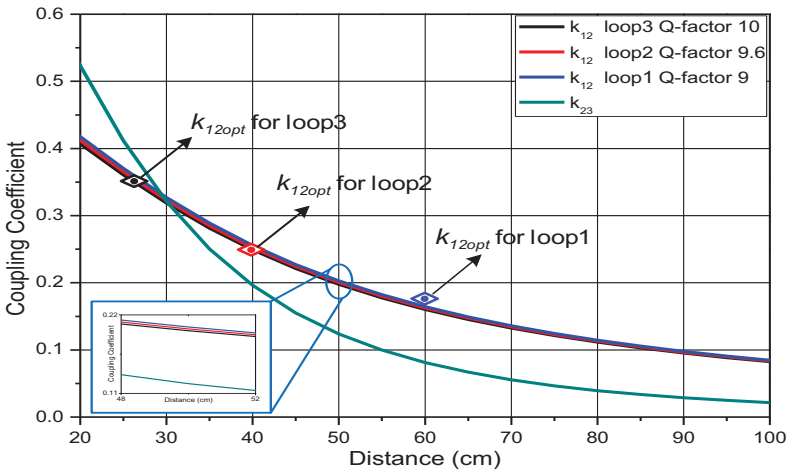

Figure 5. Computed k_{12opt} for the Case 2 system for three different loops and k_{23} for varying d_{23}. The obtained k_{12} for different loops are indicated with three points.

The system is simulated with the Agilent ADS (Advanced Design System) tool for the theoretical verification. The circuit simulation is performed with the extracted parameters from the measurement Table 2 and the computed k_{12} and k_{23} parameters. Figures 6 and 7 illustrate the S_{21} magnitude of the system for Case 1 at a 13.56-MHz input frequency, with respect to coupling coefficient k_{23} and distance d_{23}. The Figures 6 and 7 indicate that one of the three loops is chosen to achieve maximum S_{21} for a particular distance. From Equation (14) and Figure 7, for the maximum efficiency up to d_{23} = 31 cm, loop3 is connected to the supply; for d_{23} > 31 cm and $d_{23} \leq 36$ cm, loop2 is connected to the supply; and for d_{23} > 36 cm, loop1 is connected to the supply. This validates that the proposed loop switching technique aids obtaining the maximum efficiency for variable distances between the transmitter and receiver.

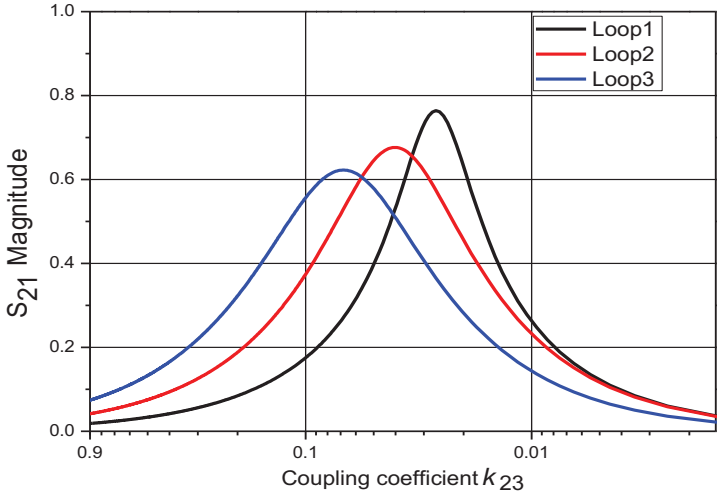

Figure 6. Simulated S_{21} magnitude for different loops with varying k_{23} in the Case 1 system.

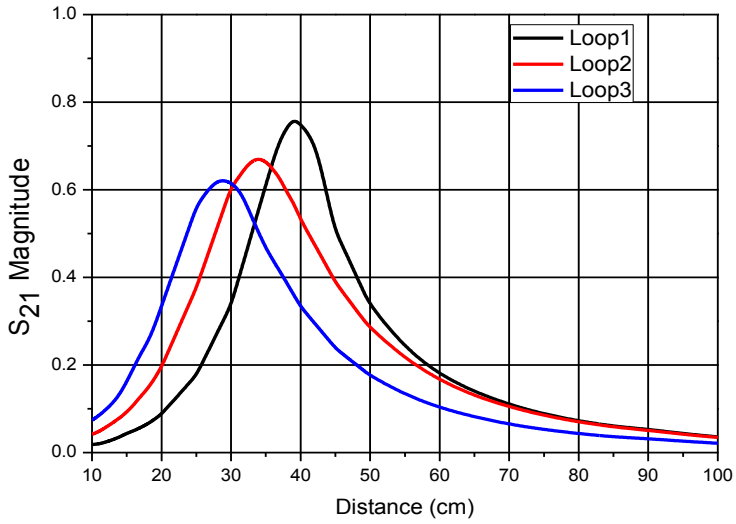

Figure 7. Simulated S_{21} magnitude for different loops with varying d_{23} in the Case 1 system.

The simulated S_{21} of the system for Case 2 with respect to k_{23} and d_{23} is depicted in Figures 8 and 9, respectively. From Equation (14) and the graph in Figure 9, maximum efficiency is derived for $d_{23} \leq 33$ cm when loop3 is connected to the supply; for maximum efficiency in the range $d_{23} > 33$ cm and $d_{23} \leq 52$ cm, loop2 is connected to the supply; and for $d_{23} > 52$ cm, loop1 is connected to the supply. The plot in Figure 9 referring to Case 2 in comparison to Figure 7 referring to Case 1 exhibits higher efficiency over a wider range of d_{23}, which validates the Case 2 system to be more effective for implementation. The resultant high efficiency can be correlated to the k_{12opt} plotted in Figures 4 and 5. It is observed that the obtained k_{12} for the three loops closely follows k_{12opt} computed in Figure 5 in comparison to the computed k_{12opt} in Figure 4. The closer the computed k_{12opt} to the obtained k_{12}, the better the efficiency obtained.

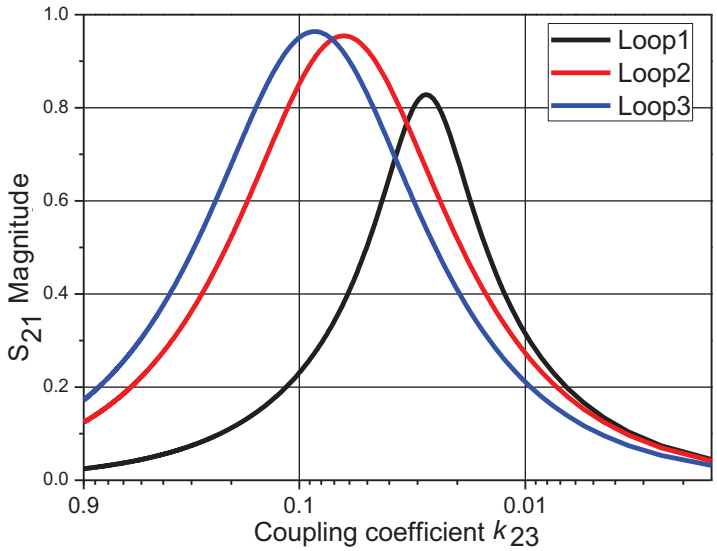

Figure 8. Simulated S_{21} magnitude for different loops with varying k_{23} in the Case 2 system.

To verify the theoretical conclusions and simulation results, the fabricated system is tested with the aid of a VNA. The S-parameter curves are measured for various d_{23}, for Case 1 and Case 2, and the measured efficiency is plotted in Figures 10 and 11, respectively. The results indicate

that the experimental results closely follow the simulation results for the S_{21} curve for varying d_{23}. The Figures 10 and 11 validate experimentally that the switched loop technique can be effectively used for obtaining maximum power transfer efficiency for varying distances between the transmitter and receiver.

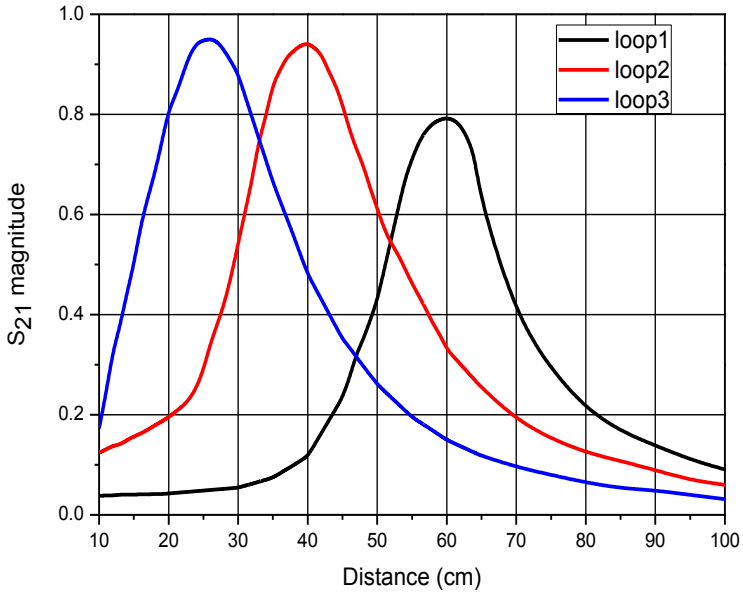

Figure 9. Simulated S_{21} magnitude for different loops with varying d_{23} in the Case 2 system.

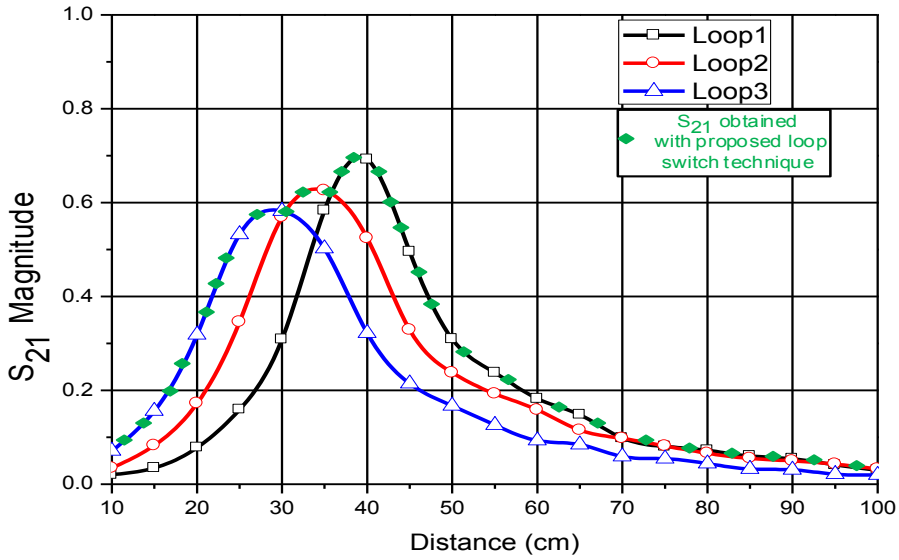

Figure 10. Measured S_{21} magnitude using a vector network analyzer (VNA) for different loops with varying d_{23} in the Case 1 system.

Figures 12 and 13 show the measured plot of transfer efficiency *versus* distance at a fixed frequency of 13.56 MHz for the Case 1 and Case 2 conditions as in Section 4. The individual loop coil efficiency is plotted along with the transfer efficiency obtained based on the switching loop technique (diamond blocks in green color) for varying d_{23}. It can be observed from the plots in Figures 12 and 13 that the measured transfer efficiency follows a similar pattern to that of the measured S_{21} magnitude depicted in Figures 10 and 11. The experimental verification is done in the same manner as the VNA measurements. The receiver side is incrementally moved away from the transmitter side

along the WPT systems' common axis to record the values. An RF power generator with a 50-Ω source resistance supplied 10 Watts of power to the transmitter, which was collected at the receiver equipped with an RF power meter with a 50-Ω load resistance.

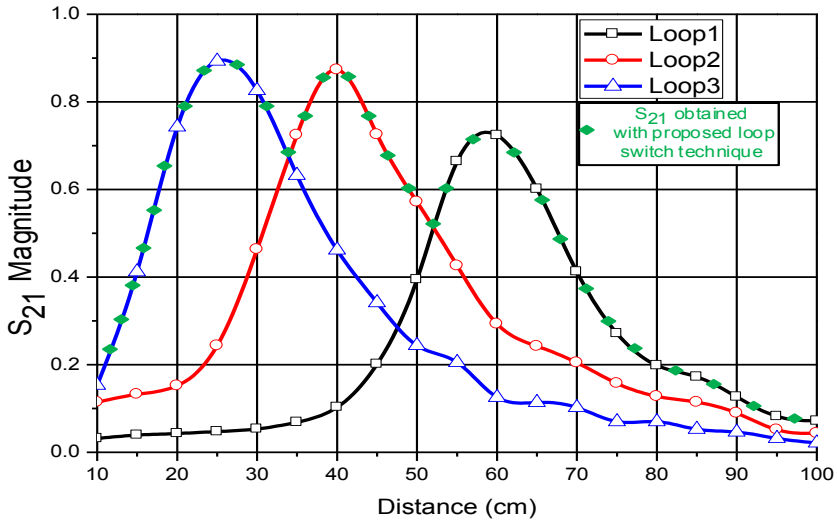

Figure 11. Measured S_{21} magnitude using VNA for different loops with varying d_{23} in the Case 2 system.

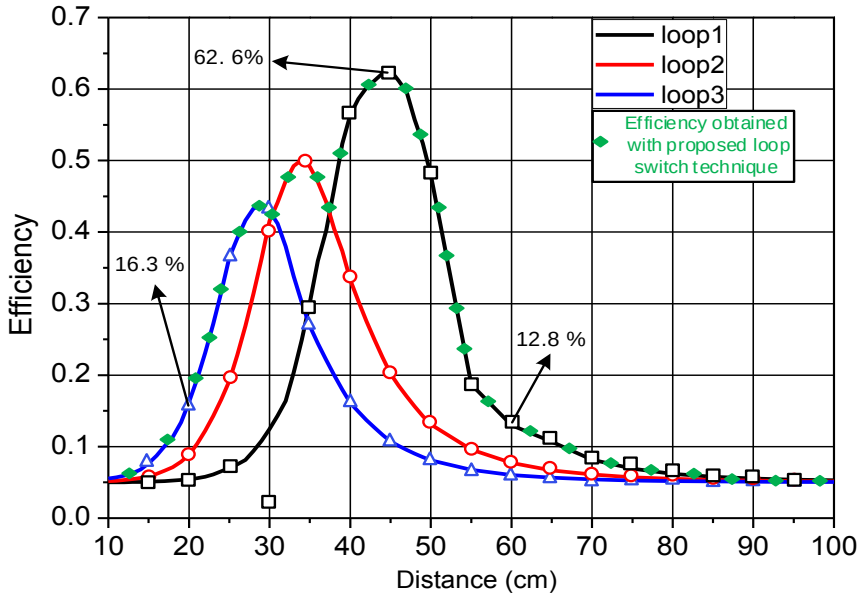

Figure 12. Measured power transfer efficiency using the RF power meter for different loops with varying d_{23} in the Case 1 system.

For the Case 1 system, from Figure 12, it is noted that the maximum efficiency (62.6%) is obtained at d_{23} = 45 cm, when loop1 is connected to the supply. At d_{23} = 20 cm, the maximum efficiency obtained is 16.2 % when loop3 is connected to the supply. For d_{23} = 35 cm, loop2 is connected to achieve the maximum efficiency of 49.8%. The power supply is switched to loop1 to obtain high power efficiency for d_{23} >37 cm. The experimental results from Figure 12 indicate that the loop coil switching technique effectively increases the efficiency of the system in comparison to the WPT system consisting of only a single source coil for varying d_{23}.

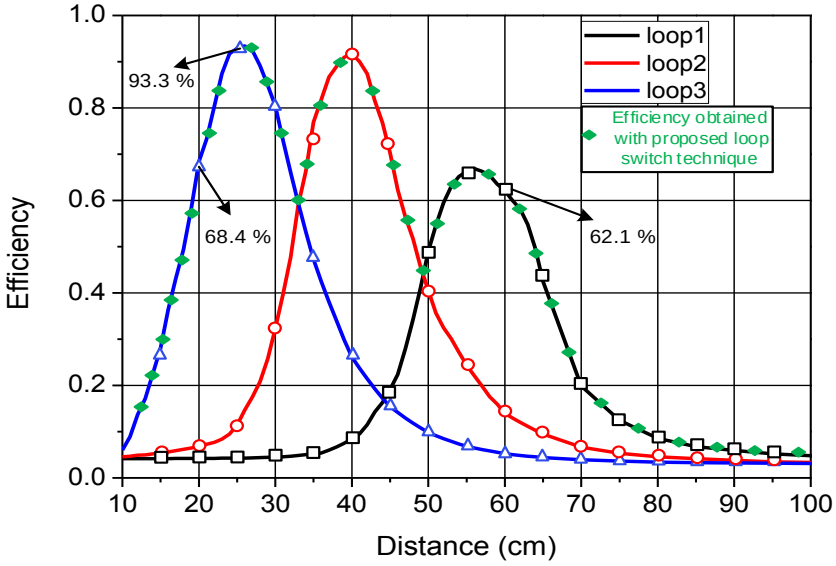

Figure 13. Measured efficiency using the RF power meter for different loops with varying d_{23} in the Case 2 system.

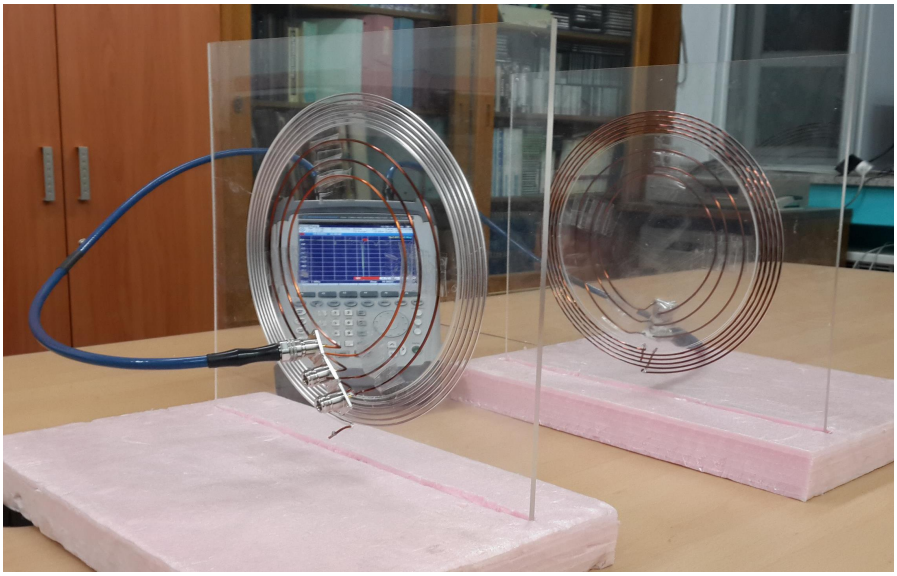

Figure 14. Fabricated resonators for the measurement analysis.

For measurement results in the Case 20-type system, the results from Figure 13 indicate that higher efficiency for a wide range of d_{23} can be obtained. The plot illustrates that a maximum efficiency of 93.3% is obtained for d_{23} = 25 cm, when loop3 is switched to the power supply. For d_{23} >32 cm and d_{23} ≤49 cm, the supply source is switched to loop2 to achieve maximum efficiency. For d_{23} >52 cm, loop1 is connected to the power source to obtain high efficiency. It is evident from Figures 12 and 13 (reference points d_{23}= 20 cm: Case 1 efficiency is 16.2%, Case 2 efficiency is 68.4%; d_{23} = 60 cm: Case 1 efficiency is 12.8%, Case 2 efficiency is 62.1%) that the two side multiple loop coil switching technique achieves higher transfer efficiency over a wide distance range, in comparison to single-sided multiple loop coil switch technique. Figure 14 shows the fabricated system for the test.

In the proposed system, loop3 is considered to be more effective for short distances (Figures 12 and 13). However, efficiency decreases rapidly after a particular distance (for d_{23} >30 cm

in Figure 12 and d_{23} >25 cm in Figure 13) as k_{23} deviates from the critical coupling point [11]. The efficiency also decreases for very short-range distances due to the occurrence of frequency splitting phenomena, as explained in [11,21]. The efficiency drops can be minimized by either employing a greater number of loops or utilizing a variable impedance matching network. However, employing an impedance matching network contributes to bulkier systems. Another technique to compensate for the efficiency loss is to adjust the supply frequency at a distance closer than the critical coupling point, so as to restrict the frequency splitting phenomena [11]. However, this technique is not suitable for implementation in standard systems, as it violates the ISM frequency band. Furthermore, a technique based on varying the k_{12} by adjusting the d_{12} and d_{34} reported in [13,18–21] improved efficiency, but the physical movement of the source and load coils is not feasible for implementation. Accounting for all of these factors, the proposed system proves to be more effective for improvising the efficiency in WPT systems. The implementation of switches in the system is mainly to demonstrate the effectiveness of the system when the system is built for adaptively switching the power to different coils as the distance between the Tx and Rx is varied. In our system, the automatic/adaptive switching algorithm has yet to be implemented.

6. Conclusions

In this paper, we proposed and designed a switched multiple loop coil technique to obtain high power transfer efficiency, for varying distances between the transmitter and the receiver for a fixed frequency. The technique involves adjusting the coupling coefficient effectively with multiple loop switching for variation in the distance between Tx and Rx. Two conditions have been analyzed: (1) the single-sided loop switch technique; (2) the double-sided loop switching technique. The system is analyzed based on the formulation of equations, and the theory is validated by supporting simulation results and experimental verification. The results indicate that the double-sided switching technique provides higher transfer efficiency over a wider range of distances. The implemented system results in being much more effective to improve the power transfer efficiency, compared to prior works based on impedance matching or automatic frequency tuning, as it is less bulky and follows the ISM band frequency specifications. The system could be implemented for various applications, like a wireless charging hub for portable electronic devices and electric vehicles.

Acknowledgments: This work was supported by Basic Science Research Program through the National Research Foundation of Korea (NRF) funded by the ministry of Education (NRF-2013R1A1A4A01012624) and the Kyungpook National University Research Fund 2015.

Author Contributions: Vijith Vijayakumaran Nair designed and tested the system. Jun Rim Choi provided guidance and key suggestions for the system design and testing.

Conflicts of Interest: The authors declare no conflict of interest.

References

1. Wei, X.C.; Li, E.P.; Guan, Y.L.; Chong, Y.H. Simulation and Experimental Comparison of Different Coupling Mechanisms for the Wireless Electricity Transfer. *J. Electromagn. Waves Appl.* **2009**, *23*, 925–934.
2. Low, Z.N.; Chinga, R.; Tseng, R.; Lin, J. Design and Test of a High-Power High-Efficiency Loosely Coupled Planar Wireless Power Transfer System. *IEEE Trans. Ind. Electron.* **2009**, *56*, 1801–1812.
3. Casanova, J.; Low, Z.N.; Lin, J. Design and Optimization of a Class-E Amplifier for a Loosely Coupled Planar Wireless Power System. *IEEE Trans. Circuits Syst. II: Express Briefs* **2009**, *56*, 830–834.
4. Nair, V.; Choi, J. An Integrated Chip High-Voltage Power Receiver for Wireless Biomedical Implants. *Energies* **2015**, *8*, 5467–5487.
5. Mutashar, S.; Hannan, M.A.; Samad, S.; Hussain, A. Analysis and Optimization of Spiral Circular Inductive Coupling Link for Bio-Implanted Applications on Air and within Human Tissue. *Sensors* **2014**, *14*, 11522–11541.
6. Lawson, J.; Pinuela, M.; Yates, D.C.; Lucyszyn, S.; Mitcheson, D.P. Long range inductive power transfer system. *IOP J. Phys.* **2013**, *476*, 16–21.

7. Pinuela, M.; Yates, D.; Lucyszyn, S.; Mitcheson, P. Maximizing DC-to-Load Efficiency for Inductive Power Transfer. *IEEE Trans. Power Electron.* **2013**, *28*, 2437–2447.
8. Kurs, A.; Karalis, A.; Moffatt, R.; Joannopoulos, J.D.; Fisher, P.; Soljacic, M. Wireless Power Transfer via Strongly Coupled Magnetic Resonances. *Science* **2007**, *317*, 83–86.
9. Karalis, A.; Joannopoulos, J.D.; Soljacic, M. Efficient wireless non-radiative mid-range energy transfer. *Ann. Phys.* **2008**, *323*, 34.
10. Imura, T.; Okabe, H.; Hori, Y. Basic experimental study on helical antennas of wireless power transfer for Electric Vehicles by using magnetic resonant couplings. In Proceedings of the Vehicle Power and Propulsion Conference, VPPC '09, Dearborn, MI, USA, 7–11 September 2009; IEEE: New York, NY, USA, 2009; pp. 936–940.
11. Sample, A.; Meyer, D.; Smith, J. Analysis, Experimental Results, and Range Adaptation of Magnetically Coupled Resonators for Wireless Power Transfer. *IEEE Trans. Ind. Electron.* **2011**, *58*, 544–554.
12. Nair, V.; Nagakarthik, T.; Choi, J.R. Efficiency enhanced magnetic resonance wireless power transfer system and High Voltage integrated chip power recovery scheme. In Proceedings of the 2014 IEEE International Conference on Electronics, Computing and Communication Technologies (IEEE CONECCT), Bangalore, India, 6–7 January 2014; pp. 1–6.
13. Duong, T.P.; Lee, J.W. Experimental Results of High-Efficiency Resonant Coupling Wireless Power Transfer Using a Variable Coupling Method. *IEEE Microw. Wirel. Compon. Lett.* **2011**, *21*, 442–444.
14. Beh, T.C.; Kato, M.; Imura, T.; Oh, S.; Hori, Y. Automated Impedance Matching System for Robust Wireless Power Transfer via Magnetic Resonance Coupling. *IEEE Trans. Ind. Electron.* **2013**, *60*, 3689–3698.
15. Koh, K.E.; Beh, T.C.; Imura, T.; Hori, Y. Impedance Matching and Power Division Using Impedance Inverter for Wireless Power Transfer via Magnetic Resonant Coupling. *IEEE Trans. Ind. Appl.* **2014**, *50*, 2061–2070.
16. Chen, C.J.; Chu, T.H.; Lin, C.L.; Jou, Z.C. A Study of Loosely Coupled Coils for Wireless Power Transfer. *IEEE Trans. Circuits Syst. II: Express Briefs* **2010**, *57*, 536–540.
17. Lee, J.; Lim, Y.S.; Yang, W.J.; Lim, S.O. Wireless Power Transfer System Adaptive to Change in Coil Separation. *IEEE Trans. Antennas Propag.* **2014**, *62*, 889–897.
18. Hui, S.; Zhong, W.; Lee, C. A Critical Review of Recent Progress in Mid-Range Wireless Power Transfer. *IEEE Trans. Power Electron.* **2014**, *29*, 4500–4511.
19. Hoang, H.; Lee, S.; Kim, Y.; Choi, Y.; Bien, F. An adaptive technique to improve wireless power transfer for consumer electronics. *IEEE Trans. Consumer Electron.* **2012**, *58*, 327–332.
20. Ahn, D.; Hong, S. A Transmitter or a Receiver Consisting of Two Strongly Coupled Resonators for Enhanced Resonant Coupling in Wireless Power Transfer. *IEEE Trans. Ind. Electron.* **2014**, *61*, 1193–1203.
21. Zhang, Y.; Zhao, Z.; Chen, K. Frequency-Splitting Analysis of Four-Coil Resonant Wireless Power Transfer. *IEEE Trans. Ind. Appl.* **2014**, *50*, 2436–2445.
22. Waters, B.J.; Sample, A.; Smith, J.R. Adaptive Impedance Matching for Magnetically Coupled Resonators. In Proceedings of the PIERS Proceedings, Moscow, Russia, 19–23 August 2012.
23. Pozar, D.M. *Microwave Engineering*, 4th ed.; Wiley: Hoboken, NJ, USA, 2012.
24. RamRakhyani, A.K.; Mirabbasi, S.; Chiao, M. Design and Optimization of Resonance-Based Efficient Wireless Power Delivery Systems for Biomedical Implants. *IEEE Trans. Biomed. Circuits Syst.* **2011**, *5*, 48–63.
25. Jow, U.M.; Ghovanloo, M. Design and Optimization of Printed Spiral Coils for Efficient Transcutaneous Inductive Power Transmission. *IEEE Trans. Biomed. Circuits Syst.* **2007**, *1*, 193–202.
26. Babic, S.; Salon, S.; Akyel, C. The mutual inductance of two thin coaxial disk coils in air. *IEEE Trans. Magn.* **2004**, *40*, 822–825.
27. Babic, S.; Sirois, F.; Akyel, C.; Lemarquand, G.; Lemarquand, V.; Ravaud, R. New Formulas for Mutual Inductance and Axial Magnetic Force Between a Thin Wall Solenoid and a Thick Circular Coil of Rectangular Cross-Section. *IEEE Trans. Magn.* **2011**, *47*, 2034–2044.
28. Nguyen, M.Q.; Hughes, Z.; Woods, P.; Seo, Y.S.; Rao, S.; Chiao, J.C. Field Distribution Models of Spiral Coil for Misalignment Analysis in Wireless Power Transfer Systems. *IEEE Trans. Microw. Theory Techn.* **2014**, *62*, 920–930.